Microchemical Journal 204 (2024) 111071

Contents lists available at ScienceDirect

Microchemical Journal

journal homepage: www.elsevier.com/locate/microc

Multi-compartmentalized electrochemical sensing platforms for monitoring cascade enzymatic reactions

Laia L. Fernández [a,b], Julio Bastos-Arrieta [c], Dietmar Appelhans [d], Yang Zhou [d], Silvia Moreno [d,*], Cristina Palet [a], Mireia Baeza [b,*]

[a] GTS Research Group, Department of Chemistry, Faculty of Science, Edifici C-Nord, Universitat Autònoma de Barcelona, Carrer dels Til·lers, 08193 Bellaterra, Spain
[b] GENOCOV Research Group, Department of Chemistry, Faculty of Science, Edifici C-Nord, Universitat Autònoma de Barcelona, Carrer dels Til·lers, 08193 Bellaterra, Spain
[c] Grup d'Electroanàlisi, Department of Chemical Engineering and Analytical Chemistry, Universitat de Barcelona, Carrer Martí i Franqués 1-11, 08028 Barcelona, Spain
[d] Leibniz-Institut für Polymerforschung Dresden e.V., Hohe Straße 6, Dresden 01069, Germany

ARTICLE INFO

Keywords:
Composite
Enzymes
Nanozymes
Hemin chloride
Nanocompartments
Polymersomes

ABSTRACT

Designing an electrochemical biosensor with the required features is a complex process involving multiple factors. For instance, nanocomposite materials used ensure the adaptation of the sensor to specific parameters on demand. But beyond making more versatile sensors, these materials likely offer excellent sensing platforms to mimic biological processes (e.g. cell communication) on the electrode surface. For this, developed methods are needed to integrate non-conductive nanoreactors for molecular communication into a biocompatible matrix on electrode surfaces with the request of spatially separated and controlled enzyme localization. Here, we present a novel reduced graphene oxide hybrid material to immobilize polymeric nanoreactors supported by an alginate network as a matrix on the electrode surface. The possibility of introducing cascade reactions in an electrochemical biosensor has the advantage of broadening the target substrates as well as their selectivity using enzymes in different nanocompartments (=compartmentalization). The polymeric vesicles allow the loading of enzymes or artificial enzymes, offering active center retention and long-term enzyme stability. Firstly, the inclusion of spatially separated polymeric active nanocompartments into the matrix on the electrode surface is used to monitor a simple enzyme reaction. However, the study's accomplishment lies in its successful ability to monitor an enzyme cascade reaction, one producing and the other consuming hydrogen peroxide, hosting natural and artificial enzymes. This proof-of-concept generates an important contribution to the design of analytical platforms capable of detecting complex environments or even monitoring communication between cell-like structures, extremely useful for fields such as synthetic biology, biomimetics and advanced biosensors.

1. Introduction

Last decades, biosensors have proven to be an innovative, emerging, and fast-growing research area playing a crucial role in healthcare, drug discovery, food safety and environmental areas. In particular, electrochemical biosensor technology is crucial in the diagnosis of relevant diseases, they can measure analytes in real-time, which is useful for monitoring rapid changes in biological fluids [1]. Converting biological information into an easily readout signal is challenging, and the overall performance of sensors is often determined by the interfaces between the sensing element and the biological sample at the nanometer scale. Electrochemical biosensors composed of nanocomposite material guarantee a suitable interface and desired features such as cost-effective, portable, and reliable devices [2,3]. These electrochemical platforms can be based on carbon allotropes that are conductors (e.g. graphite, carbon nanotubes (CNTs), reduced graphene oxide (rGO), etc.) and a polymeric matrix (e.g. Epoxy, Teflon, etc.) which is an insulating material, both maintaining their properties. A suitable approach to obtain the optimum ratio between the carbonaceous conductive material and the polymeric matrix is the use of percolation curves. It provides the data necessary to find a compromise between the relation of signal/noise ratio and the percentage of conductive material needed to obtain an improved analytical signal. The optimal percentage for graphite sensors (15 %) was previously investigated [4].

* Corresponding authors.
E-mail addresses: moreno@ipfdd.de (S. Moreno), mariadelmar.baeza@uab.cat (M. Baeza).

https://doi.org/10.1016/j.microc.2024.111071
Received 28 December 2023; Received in revised form 8 May 2024; Accepted 24 June 2024
Available online 25 June 2024

Besides that, the addition of nanomaterials to an optimized sensor composition offers exciting possibilities for enhancing assay sensitivity, but also broadening the scope for studying complex matrices or even metabolites involved in biological reactions. For instance, liposomes have played a key role in the development of biosensing assays due to their similarities with cell membranes. Thus, they are widely used in protein-membrane interaction studies, in membrane protein biosensing and drug discovery research [5].

On the other hand, polymeric material science has evolved to develop synthetic nanostructures called polymerosomes (polymeric vesicles), capable of hosting active bio(macro)molecules and regulating their activity/function through their membrane permeability [6,7]. These structures consist of self-assembled amphiphilic block copolymers offering greater versatility and membrane stability compared to liposomes [7]. Particularly, stimuli-responsive polymeric vesicles possess the ability to load enzymes which makes them very suitable as nanoreactors capable of performing enzymatic reactions in local environments (compartmentalization) under different external stimuli (pH change, potential/current, light, ionic strength, etc.) and also enhancing the enzyme stability [6,8–10]. Natural enzymes (NEs) have been loaded into polymeric vesicles and have also been used in the sensing field [11]. Enzymatic biosensors possess high selectivity but have always suffered from limitations such as instability, complicated modification procedures, and critical microenvironmental factors. These limitations can be overcome by using these polymeric nanoreactors through the stabilization effect of the polymeric environment [8,11].

Modification of bare electrode surfaces using nanocomposite materials comprising nanomaterials and polymer matrices exploits the intrinsic properties of both components [12]. However, the response characteristics of electrochemical sensors are strongly influenced by the properties of the transducer material and its functionalization with different nanomaterials. For instance, polymeric vesicles are made of non-conductive block copolymers, and their immobilization could affect their morphology, mechanical stability, and stimuli-responsiveness. Therefore, the use of carbon materials, such as CNTs or rGO, presents a strategic solution to this issue. These carbon materials are well-known conductive biocompatible materials that can be easily customized chemically to increase the affinity of the charged polymeric vesicles, finally, to anchor loaded polymeric vesicles to the electrode surface [13–15].

Previously, pH-responsive and photo-crosslinked polymeric vesicles (Psomes) have shown their potential as smart nanoreactors [16–20]. Different types of enzyme-loaded Psomes have been established mainly by an *in situ* loading method, which allows to regulate their enzymatic capacity through membrane permeability, promotes a compartmentalized enzymatic cavity, cascade reactions, and above all, improves enzyme stability [16,19,20]. Moreover, the incorporation of artificial enzymes (or nanozymes = NZs) such as hemin molecules into the mentioned Psomes has also been reported, allowing enzyme-like properties to be established in the cavities of Psomes [21].

This work aims to develop a sensing platform based on the incorporation of hybrid nanocomposite structures, such as polymeric nanoreactors, into electrochemical biosensors leading to the detection of electro-active products obtained by an enzymatic reaction. The goal of this integration is to enhance the performance of the sensors through synergistic properties and to extend their utility to other domains, such as biomimetics. Biomimetics is a field that seeks to imitate and monitor complex biological processes, making it highly relevant to this research. Here we have successfully established a sensing platform where model enzyme cascade reactions take place at the interface between different polymeric nanocompartments. This accomplishment serves as a proof of concept and significantly advances our ability to mimic multi-compartmentalized biological processes monitored by an electrochemical technique such as chronoamperometry. For this purpose, rGO modified with gold nanoparticles (AuNPs) and β-cyclodextrin (β-CD-AuNPs@rGO) was used to anchor different Psomes-based nanoreactors [22], previously embedded in an alginate (AL) network to the electrode surface (Scheme 1A). The structure and enzymatic properties of the loaded Psomes were confirmed using dynamic light scattering (DLS), cryogenic transmission electron microscopy (cryo-TEM) and fluorescence techniques. The surface of the entire modified electrode was characterized by scanning electron microscopy (SEM). To provide the enzyme function in the modified electrode, glucose oxidase-(GOx)-loaded Psomes (GOx-Psomes) were used as a model nanoreactor, along with the GOx-like properties of AuNPs acting as a symbiotic biosensor. The production of H_2O_2 from both components in the presence of glucose (intravenous glucose solution) was monitored. Subsequently, to achieve the proposed goal, we further modified the electrode by combining two antagonistic nanocontainers, one nanocontainer producing H_2O_2 (GOx-Psomes) and one nanocontainer consuming H_2O_2, promoting a cascade reaction at the interface. The second nanocontainer was based on either a NE such as catalase (CAT-Psomes) or a NZ such as hemin molecule ($(\beta CD)_2$Hemin-Psomes) (Scheme 1B). This research contribution not only advances the development of heterogeneous and multi-compartmentalized sensing platforms but also introduces the usage of biologically-like active artificial cavities such as NZs, thereby improving the cost-effectiveness and durability of advanced sensing devices.

2. Experimental

2.1. Materials

Poly(ethylene glycol) methyl ether (Me-PEG-OH; M_n = 2000 g mol^{-1}), 2,2′-bipyridine, 4-aminobutanol, 2-(*N, N*-diethylamino)ethyl methacrylate (DEAEMA), methacryloyl chloride, 2-bromoisobutyryl bromide, 2-aminoethanol, copper-I-bromide, aluminum oxide (neutral, activated), ferricyanide/ferrocyanide (99.8 %), 4-amino-1-butanol (98 %), phosphate buffered saline (tablet), sodium alginate (M_w = 10000–60000 g mol^{-1}), sodium hydroxide, glucose oxidase from *Aspergillus niger* (GOx, essentially salt-free, lyophilized powder), ethanol (99.8 %), hydrogen peroxide solution (30 %, enzyme assays), potassium chloride (99.5 %), catalase from bovine liver, myoglobin from equine skeletal muscle (95–100 %, essentially salt-free, lyophilized powder), sodium chloride, D-(+)-glucose, graphite powder, hydrochloric acid (37 %) and gold(III) chloride trihydrate ($HAuCl_4{\cdot}3H_2O$, ≥ 99.9 %), were purchased from Sigma-Aldrich (MO, USA). 3,4-Dimethylmaleic acid anhydride, anhydrous tetrahydrofuran (THF), ethyl acetate and chloroform-d (99.8 %) were purchased from Acros Organics (Geel, Belgium). *n*-Hexane, hydrochloric acid (37 %), triethylamine, H_2O_2 (30 %, electroanalytical measurements), ethanol (≥ 99.8 %) and silica gel were purchased from Merck (Merck KGaA, Darmstadt, Germany). Sodium nitrate ($NaNO_3$, 99 %), sodium borohydride ($NaBH_4$, Analytical grade) and potassium permanganate ($KMnO_4$, ≥ 99.5 %) from Labkem (Labbox Labware, S.L., Barcelona, Spain). Sulfuric acid (H_2SO_4, 95–97 %) from Scharlab S.L (Barcelona, Spain). Calcium carbonate ($CaCO_3$, ≥ 99 %) from Fluka. Calcium chloride ($CaCl_2$, >97 %) from Panreac Química S.L.U., (Barcelona, Spain). Anhydrous 2-butanone (Fluka), triethylamine (Fluka) and anhydrous THF (Sigma-Aldrich) were stored over a molecular sieve. Nylon filters (0.2 and 0.8 μm) and dialysis membrane Spectra/Por Biotech (CE MWCO 1000 and 100 kDa) were purchased from Carl Roth. All solutions were prepared using deionized water from the Milli-Q system (Millipore, Billerica, MA, USA) with a resistivity value of 18.2 MΩ·cm, otherwise, they were prepared in the media indicated. Heptakis-(6-deoxy-mercapto)-β-cyclodextrin (β-CD, AraChem, Tilburg, Netherlands). 40 % hypertonic glucose serum (Fresenius Kabi, Barcelona, Spain). Amplex™ Red Reagent was purchased from Life Technologies Corporation (Thermo Fisher, Eugene, USA).

2.2. Fabrication and characterization of the electrochemical biosensor

Details of the block copolymer (BCP) synthesis (Section 2) and

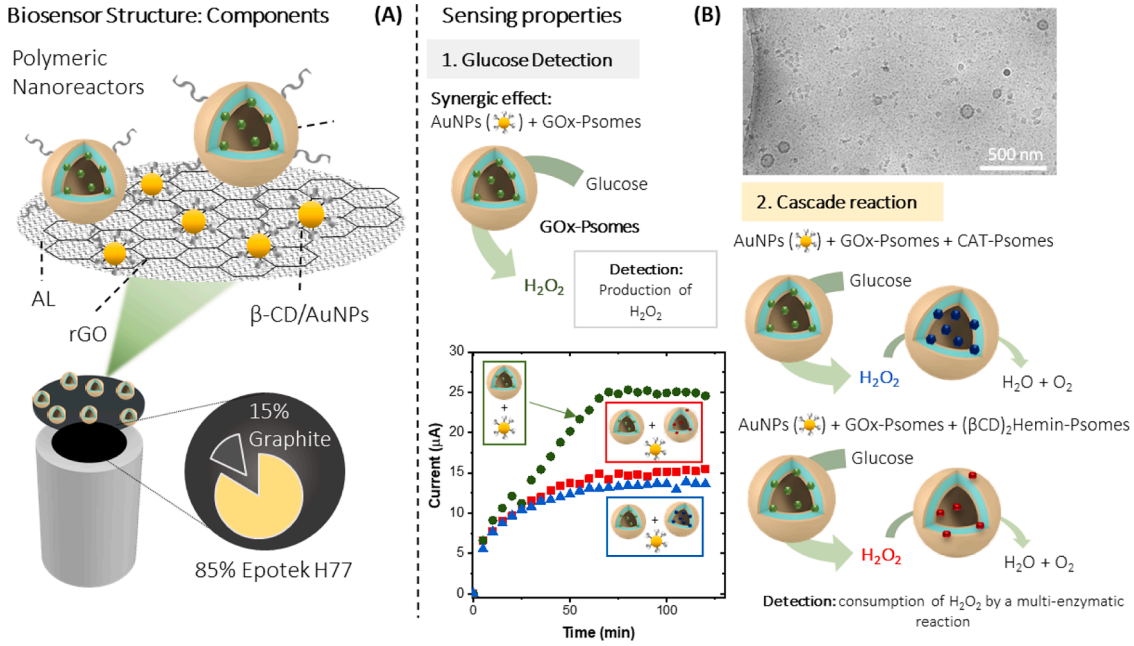

Scheme 1. (A) Schematic structure of the electrochemical biosensor. (B) Proof of concept of the sensing properties: (1) Glucose detection: β-CD-AuNPs@rGO electrode with a unique type of integrated polymeric nanoreactor (GOx-Psomes) capable of generating H_2O_2 in the presence of glucose in combination with the GOx-like properties of the AuNPs (synergistic effect); (2) Cascade Reaction: β-CD-AuNPs@rGO electrode with two different integrated polymeric nanoreactors (GOx-Psomes and CAT-Psomes or $(\beta CD)_2$Hemin-Psomes) capable of proving the cascade reaction on the electrode surface by using natural or artificial enzymes as H_2O_2-consuming nanocontainers.

characterization (Table S1) [23], self-assembly of BCPs (Section 3) [18,23], and cargo loading into Psomes (Section 4) [16–19] are shown in the Supporting Information (SI). Although two different batches of BCPs were used throughout the work, the majority of the electrochemical measurements were carried out with the second batch, which ensures the reproducibility of the electrode fabrication. The fabrication and characterization of three different loaded-Psomes (GOx-Psomes, CAT-Psomes and $(\beta CD)_2$Hemin-Psomes) are described in the SI (Figs. S1–S12; Table S2-4).

2.2.1. *AuNPs@rGO synthesis*

rGO was produced following a slightly modified Hummers' method, which implies a change in the reduction stage. At the same time, the reduction of the graphene oxide (GO) and the gold ion in a common reaction solution was carried out to realize the desired hybrid material, AuNPs@rGO.

For the rGO production, 1 g of graphite powder, 0.5 g of $NaNO_3$ and 23 mL of H_2SO_4 were added to a 500 mL round bottom flask and stirred. Then, the flask was cooled down in an ice bath due to the exothermic reaction. After, 3 g of $KMnO_4$ were slowly added to the flask and, subsequently, the solution was heated up to 45 °C for 30 min, which helped the oxidation process. The chemical process can be validated visually, the oxidised material changes colour from black to dark brown. The solution was cooled down to room temperature. Next, 46 mL of Milli-Q water were slowly added to reduce the acidity of the medium and stirred for 15 min. Later, 140 mL of Milli-Q water were added, and the solution was transferred to a beaker. Then, 3.5 mL of H_2O_2 (30 %) were added to remove the excess MnO_2 formed. The solution was washed with 10 % HCl and centrifuged at 3500 rpm as many times as necessary to remove a greenish viscous gel (MnO_2) from the supernatant. The solid product (GO) was washed with Milli-Q water and centrifuged until pH 6 was reached and was dried at 80 °C for 24 h. The resulting dark solid was milled using an agate mortar [24,25]. Then, 250 mL of 1 mg mL^{-1} GO solution were prepared and sonicated for 1 h. Ultrasonic probe model Vibracell VC50 (from Sonics & Materials INC, Newtown, CT, USA) was used. After that, 0.709 g of $HAuCl_4 \cdot 3H_2O$ and 250 mL Milli-Q water were added to the GO solution, therefore, the final concentration of the $HAuCl_4$ ended in 0.0036 M. 250 mL of $NaBH_4$ solution (0.1 M) were put in gently, drop by drop, then the solution was stirred for 1 h. Finally, the final product was centrifuged at 3500 rpm and washed with Milli-Q water until a neutral pH was obtained. A centrifuge (Digicen CE 07) with an angular rotor (RT 018) from ALRESA (Daganzo de Arriba, Madrid, Spain) was used. The resulting solid was dried at 80 °C for 24 h, yielding 132 mg (53 %) of the desired product, and then ground in an agate mortar (Labbox Labware, S.L., Barcelona, Spain). The milled AuNPs@rGO was stored at room temperature and in a dry place protected from light.

2.2.2. *Modification of AuNPs@rGO with β-cyclodextrin*

The synthesis of β-CD-AuNPs@rGO is adapted from a previous work [24]. 1 mg mL^{-1} solution of AuNPs@rGO was prepared using the ultrasound treatment for 4 h. A Heptakis-(6-deoxy-mercapto)-β-cyclodextrin (β-CD-SH) solution (2.25 mM) in 10 % ethanol was prepared. Equal volumes, 25 mL of each solution were mixed and stirred overnight. This was followed by three washing steps using the 10 % ethanol solution and centrifugation (3500 rpm for 10 min). The solid was dried at 40 °C for 3 days. It was stored at room temperature and in a dry place protected from light.

2.2.3. *Loaded-Psomes β-CD-AuNPs@Rgo*

500 μL of 3.1 mg mL^{-1} β-CD-AuNPs@rGO solution and 500 μL of 1.0 mg mL^{-1} loaded-Psomes solution (loading efficiency depending on the cargo) were in contact for 24 h with constant stirring in a 1.5 mL Eppendorf tube at room temperature. In Table S7 a list of all the compositions tested and the nomenclature used is shown.

2.2.4. *Composite electrode fabrication and modification*

For the handmade composite electrode fabrication, graphite (particle size 50 μm, Merck Millipore, Darmstadt, Germany) as the conductive material and Epotek H77A and H77B (Epoxy Technology Billerica, MA, USA) as the non-conductive polymeric matrix. Electrodes were prepared according to the established method from a previous work [3]. The ones

used in this study contained 15 % graphite and 85 % polymeric matrix. A 1 mL solution containing 250 μL of 1 % sodium alginate (Mw 10,000–60,000 g mol^{-1}), 500 μL of 1 % $CaCO_3$ and 250 μL of the nanocomposite (loaded Psomes-β-CD-AuNPs@rGO) was prepared. Then, 50 μL of this solution were taken and placed by drop-casting over the electrode. The second step was to immerse the electrode surface in 50 mL of 1 % $CaCl_2$ solution for 30 s to have an external gelation [26]. Finally, an internal gelation of the electrode nanocomposite was performed by applying 1.5 V for 15 min [27]. All the hybrid materials tested are summarized in Table S7 from Section 6 of the SI. Electrode modifications were characterized using SEM-EDX, (MerlinFE-SEM from Carl Zeiss Microscopy (GmbH, Oberkochen, Germany) and EDS Oxford LINCA X-Max detector from Jeol, (Peabody, MA, USA)). The surface of the electrode was dried in the air overnight in a laminar flow chamber. Au content of 1 mg of dry solid of AuNPs@rGO or GOx-Psomes-β-CD-AuNPs@rGO was determined by using an inductively coupled plasma optical emission spectrometer 5900 from Agilent (Santa Clara, CA, USA) with a microwave digester, model ultraWAVE (Milestone Srl, Sorisole, Italy).

2.3. Electrochemical characterization and electroanalytical measurements

Electrochemical measurements were performed using EmStat 4 s (Palmsens B.V, Houten, The Netherlands). Three electrode configurations were used: a platinum electrode 53–671 (Crison Instruments, Alella, Barcelona, Spain) as a counter electrode, an Ag/AgCl Orion 900 single-junction electrode filled with a reference filling solution Orion 900,001 (Thermo Electron Corporation, Beverly, MA, USA) as a reference electrode, and the modified composite electrodes were used as working electrodes. Furthermore, due to the permeability of the membrane of the commercial electrode to the $[Fe(CN_6)]^{3-}/[Fe(CN_6)]^{4-}$ solution, a homemade Ag/AgCl electrode was used for characterization.

2.3.1. Electrochemical characterization

The cyclic voltammetry (CV) measurements were carried out in a quiescent state and with a solution composed of 0.1 M KCl, using an equimolar mixture of ferricyanide/ferrocyanide, 0.01 M $[Fe(CN)_6]^{3-}/[Fe(CN)_6]^{4-}$. Phosphate buffered saline 10 mM at pH 7.4 (PBS, from tablets) was employed for CV measurements. Also, 4×10^{-5} and 7×10^{-5} M solutions of glucose were prepared in PBS. All the measurements were performed at a fixed scan rate of 10 $mV \cdot s^{-1}$.

2.3.2. Electroanalytical measurements

The chronoamperometric measurements were carried out every 5 min for 60 s at 1.4 V if it is not noted otherwise. For data processing, ten points were selected from second 29 to second 30; data points correspond to the period where the signals are stable (Fig. S13). The average was calculated and shown in this work. The range of concentration used for the calibration curves was from 2×10^{-5} to 3×10^{-4} M of glucose in 10 mM PBS at pH 7.4.

2.3.3. Application to real samples

Sample analysis was performed by standard addition calibration and the technique explained above. Two different kinds of samples were investigated: (i) commercial 40 % hypertonic glucose serum: firstly, 2 mL of intravenous glucose solution in 250 mL of PBS 10 mM at pH 7.4 to make the stock solution. Then, 1 mL was taken from the previous solution and diluted in 100 mL of PBS 10 mM at pH 7.4; (ii) synthetic samples were prepared in PBS 10 mM at pH 7 by the addition of glucose, 1 mL glucose stock 0.004 M in 25 mL PBS. This kind of sample was measured directly. The reference method to compare the results was a bioanalyzer YSI 2700 Select from Marshall Scientific (Hampton, NH, USA). The measurements were made by triplicate for each sample and the average of them was compared to the results obtained in this work. The working pH was set at a pH of 7.4, unless otherwise specified. The solutions used for pH adjustment consisted of 0.1 M NaOH (98 % Alfa Aesar, from Thermo Fisher Scientific, Kandel, Germany) and 1 M HCl (37 %, Sigma Aldrich St. Louis, MO, USA), using an HI 2211 pH/ORP meter. The calibration solutions were supplied by Hanna Instruments S. L, (Eibar, Gipuzkoa, Spain).

3. Results and discussion

3.1. Synthesis and characterization of polymeric nanoreactors

pH-responsive and crosslinked Psomes were used to fabricate polymeric nanoreactors based on previous works [17,18]. The used block copolymer $mPEG_{45}$-b-P(DEAEMA-co-DMIBMA) (BCP) was synthesized by atom transfer radical polymerization (Table S1, more details SI) [17]. The preparation method of GOx-Psomes and CAT-Psomes was adopted from previous reports by using an *in situ* loading approach (Fig. S3) [16–19,28]. Size distribution, pH-responsiveness and stability of both Enzyme-Psomes were investigated by DLS. Cyclic pH switches of Enzyme-Psomes were performed at pH 8.0 (collapsed state) and 5.0 (swollen state) proving no disassembly and membrane rupture as well as no aggregation (Fig. S1, S4 and S7). The morphology (vesicular structure) and diameter were confirmed by cryo-TEM. The resulting particle sizes (∅GOx-Psomes = 72 ± 15 nm; ∅CAT-Psomes = 70 ± 16 nm) and membrane thickness (MTGOx-Psomes = 18.9 ± 3.2 nm; MTCAT-Psomes = 16.7 ± 3.3 nm) are in the range of previously published results (Fig. S6 and S9) [16,18,19]. A pH titration was carried out by determining the pH* value (semi-open state) [16] to obtain pH* values in the range of 6.5–6.9 (Fig. S2, S4 and S7). However, this parameter is strongly dependent on the Psomes concentration, its value could be (slightly) different for Enzyme-Psomes in nanocomposite layers. Labelled enzymes were used to estimate the loading efficiency ($L.E_{GOx}$ = 27 %, 0.05 mg mL^{-1} and $L.E_{CAT}$ = 24 %, 0.05 mg mL^{-1} per 1.0 mg mL^{-1} BCP, Fig. S5 and S8). Relatively higher loading efficiencies than previously reported have been obtained (<10 % for GOx, for CAT no previous data) [18,29]. This can imply a higher integration of the NEs into the membrane. The enzyme activity of GOx-Psomes and CAT-Psomes were studied in solution by using the Amplex Red assay. Higher activities can be observed when the Psomes membrane is in an open state (=swollen state). Moreover, notable activities are also given by the collapsed state of the Psomes membrane (Fig. S12). This observation leads us to the conclusion that both NEs are not only localized within the lumen but are also anchored to the membrane. This anchoring reduces the capacity to regulate enzyme activity in response to changes in membrane permeability. In essence, notwithstanding the closed state of the Enzyme-Psomes, the enzymes bound to the membrane can still catalyze substrates. Similar scenarios have also been reported with other enzymes [18,20,28]. In any case, the enzymatic assay probed the production and consumption of H_2O_2 in solution by GOx-Psomes and CAT-Psomes (Fig. S12). For the fabrication of $(\beta CD)_2$Hemin-Psomes, the recently published protocol was used by using *post* loading approach (Fig. S10, L.E $(\beta CD)_2$Hemin = 0.018 mg mL^{-1} per 0.5 mg mL^{-1} BCP) [21]. The morphology and diameter were also confirmed by cryo-TEM (∅$(\beta CD)_2$Hemin = 90 ± 25 nm; MT$(\beta CD)_2$Hemin = 28 ± 8 nm). The increase in diameter in comparison with Enzyme-Psomes can be attributed to the fact that two different batches of BCPs were used. However, it should be noted that the membrane is thicker. Therefore, it can be assumed that a significant amount of $(\beta CD)_2$Hemin is incorporated into the membrane (Fig. S11).

3.2. Fabrication and morphological characterization of electrochemical biosensor

The next step was the preparation of hybrid materials to modify the surface of the composite electrodes. Each component has its corresponding function: (i) AL, to improve the immobilization efficiency of the hybrid nanomaterial on the electrode surface; (ii) AuNPs@rGO, to

enhance the low conductive properties of the Psomes; (iii) β-CD units, to enhance the interaction between the electrode interphase and Psomes by physical interactions [22]. Psomes also provide a protective environment for the enzymes in the crosslinked AL matrix on the electrode surface. This intricate nanomaterial was characterized by different tools to gain an understanding of its properties. The mapping of Au in the (electrode) nanocomposites (Fig. 1A and B) indicates a high presence of this metal confirmed by ICP-OES study. Thus, Au in AuNPs@rGO presented 49 ± 15 % mass while Au in GOx-Psomes-β-CD-AuNPs@rGO was only 7.0 ± 0.7 % mass. The ICP analysis was performed without any prior treatment, using dry solid nanomaterials. The differences between the AuNPs@rGO and the GOx-Psomes-β-CD-AuNPs@rGO are attributed to the distinct steps involved in their preparation. AuNPs@rGO was synthesized according to the established protocol, and a sample was taken and analyzed by ICP-OES. For the second hybrid nanomaterial, the AuNPs@rGO was first modified with SH-β-CD and subsequently functionalized using the GOx-Psomes. Consequently, the double functionalization of AuNs@rGO leads to an increase in the mass of the final hybrid nanomaterial. This leads to a decrease in the Au mass percentage in GOx-Psomes-B-CD-AuNPs@rGO. However, a direct comparison of the two electrode surfaces (Fig. 1A and B) is difficult due to the increased complexity of the nanocomposite in the second case. This complexity may introduce additional interactions that contribute to the lower AuNPs content observed. As a result, a direct comparison of the two functionalization approaches is not feasible. From the SEM study (Fig. 1C) AL matrix presents a rugose surface after all the gelation steps. The presence of AuNPs (Fig. 1D and E; and G and H), were confirmed by the EDX study (Fig. 1F and I).

3.3. Electrochemical characterization

$[Fe(CN_6)]^{3-}/[Fe(CN_6)]^{4-}$ redox probe was used for the electrochemical characterization using CV. All kinds of modifications were investigated (Fig. 2A). The modifications containing AuNPs@rGO showed an improvement of the current towards the bare electrode. On the other hand, when this material was modified with β-CD and loaded-Psomes, the current decreased slightly. Therefore, the presence of β-CD and loaded-Psomes on the hybrid material is compensated by the AuNPs@rGO. The method provides information about the electroactive area (*A*) of the sensor and the charge transference resistance (R_{CT}). *A* was estimated using the *Randles-Sevčik* equation which is appropriate for the electron-transfer controlled process [30]:

$$I_p = 3.01 \times 10^5 \cdot n^{3/2} \cdot (\alpha v D_{Red})^{1/2} \cdot A \cdot C^*_{Red} \quad (1)$$

where *n* is the number of electrons participating in the redox process (n = 1 for ferrocyanide/ferricyanide); α corresponds to the transfer coefficient, which is approximately 0.5; and D_{red} is 6.32 x 10^{-6} $cm^2 \cdot s^{-1}$ and corresponds to the diffusion coefficient of the reduced species. The scan rate (v) is 0.01 $V \cdot s^{-1}$ and the bulk concentration of the electroactive species (C^*_{Red}) is equal to 0.01 M.

The R_{CT} was calculated using the Tafel diagrams (Fig. 2B), which give information about the reversibility of the process. The Tafel diagram represents the logarithm of the measured current versus the applied potential. In these diagrams, the exchange current (i_0) is related to the reversibility of the electrochemical process and can be applied to calculate R_{CT} [31]:

$$i_0 = RT/nFR_{CT} \quad (2)$$

In Eq. (2) *R* is the universal gas constant ($atm \cdot L \cdot K^{-1} \cdot mol^{-1}$); *T* is the temperature (K); *n* is the number of exchanged electrons ($n = 1$ for the ferrocyanide/ferricyanide redox pair) and *F* ($C \cdot mol^{-1}$) is the Faraday constant. The electroactive surface of all the intermediate-modified electrodes and R_{CT} were calculated. All this information is collected in Table 1.

All the electrode modifications present similar electroactive areas,

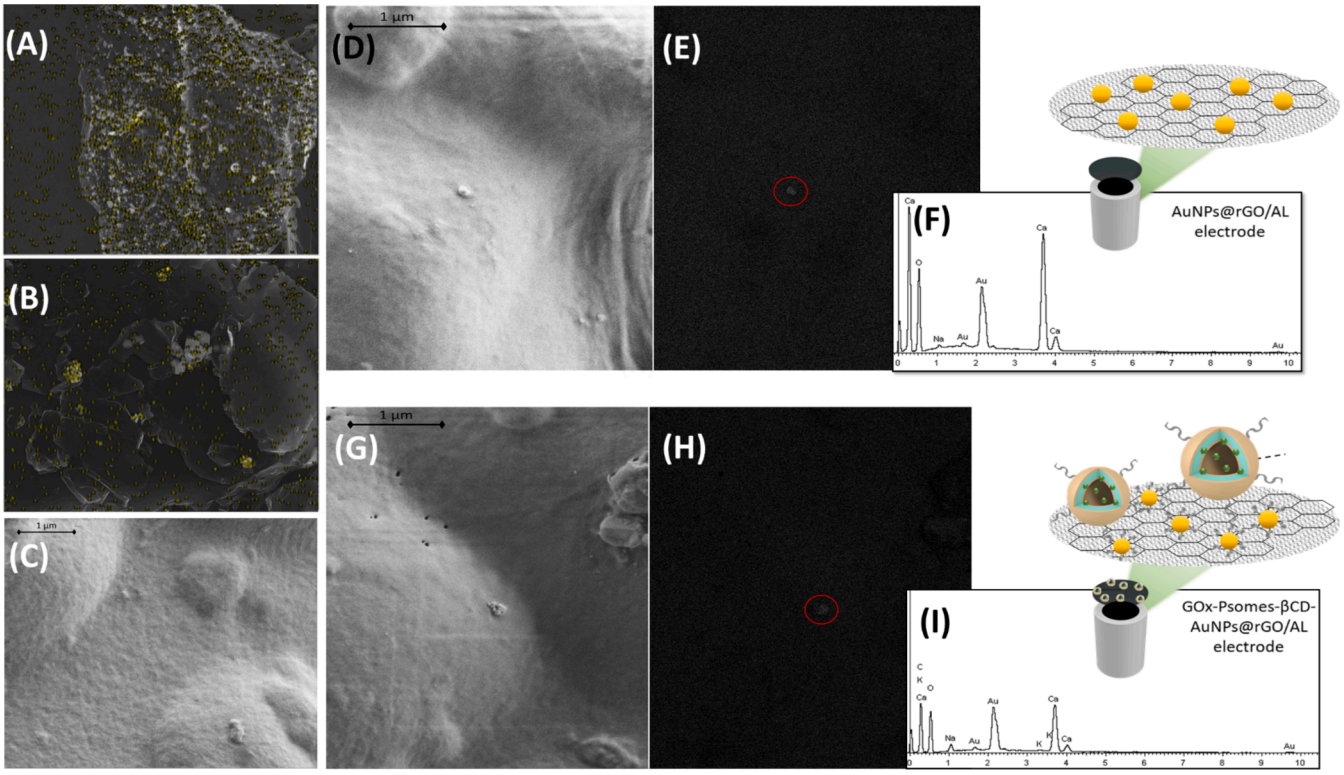

Fig. 1. SEM images: mapping of Au (yellow) of (A) AuNPs@rGO and (B) GOx-Psomes-β-CD-AuNPs@rGO. (C) Secondary electron SEM image of AL. AuNPs@rGO/AL electrode: (D) secondary electron SEM image, (E) retrodispersive and (F) EDX graph. GOx-Psomes-β-CD-AuNPs@rGO/AL electrode: (G) secondary electron SEM image, (H) retrodispersive and (I) EDX graph.

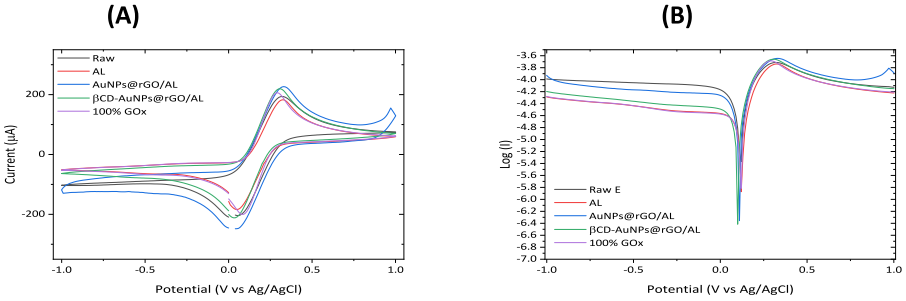

Fig. 2. Electrochemical characterization of the modified electrodes. (A) Cyclic voltammetry and (B) Tafel diagrams of different types of electrode modification. Measurements were carried out using an equimolar mixture of ferricyanide/ferrocyanide, 0.01 M $[Fe(CN)_6]^{3-}/[Fe(CN)_6]^{4-}$ in 0.1 M KCl, at a scan rate of 10 mV·s^{-1}.

Table 1
Electroactive electrode areas and R_{CT} are determined by each type of electrode functionalization.

Electrode	A [cm^2]	R_{CT} [Ω]
Raw (15 % graphite)	0.36	6707.82
Alginate (AL)	0.34	8564.09
AuNPs@rGO/AL	0.43	8216.39
β-CD-AuNPs@rGO/AL	0.40	8324.94
100 % GOx	0.38	9357.96

except for the AuNPs@rGO/AL electrode (0.43 cm^2). This difference and the lower R_{CT} (8216.39 Ω) are mainly related to the partial modification of the conductor with metal nanoparticles and rGO. This can improve the conductivity of the material. For β-CD modified AuNPs@rGO electrode, the resistance to the charge transfer increases. Thus, the potential of conductive material on the electrode surface slightly decreases. When comparing the raw electrode (15 % graphite) response with just the crosslinked AL matrix electrode response, it seems that the AL matrix on the electrode surface does not influence the electroactive area. However, it does not improve electronic transfer. Furthermore, the complete modification with GOx-Psomes also increases the R_{CT}. Thus, this modification does not enhance the flow of electrons through the nanocomposite. In summary, the R_{CT} of the electrode generally increases with some variation after each modification step of the raw electrode. The modification with AuNPs@rGO/AL outlines the lowest R_{CT} of the electrodes, while the last modification step with GOx-Psomes provides the highest R_{CT} value, due to the addition of non-conductive material.

3.4. Optimization of measurement conditions and real sample application

Following, operational electrochemical measurements were optimized considering parameters such as working potential, diffusion layer control, pH medium, response time, reproducibility, and percentage (%) of GOx-Psomes in the hybrid nanomaterial. CV in 10 mM PBS at pH 7.4 in the presence of glucose substrate was performed to determine the response of the sensing platform for the different nanocompositions on the electrode surface (Fig. S14A and Fig. S14B). To optimize the working potential for a 100 % GOx-Psomes sensor, a CV in 10 mM PBS at pH 7.4 (as a blank signal, residual current and H_2O oxidation) in the absence and presence of glucose was performed and it is shown (Fig. S14C). Thus, the higher response for the nanocomposite on the electrode surface in the presence of glucose was validated for the 100 % GOx-Psomes sensor (Fig. S14B). Next, the working potential of 100 % GOx-Psomes sensors at different glucose concentrations was tested. The difference in the response at different potentials is summarized in Fig. 3A. The potential 1.4 V outlines the best performance and higher currents. Moreover, for all potentials, a saturation zone is given over a higher glucose concentration. Hence, the 1.4 V as potential was selected for chronoamperometry experiments. Chronoamperometry can be used with or without stirring during the measurement. In Fig. 3B, the results indicate that the constant gentle stirring results in a better analytical response because of a constant diffusion layer thickness over the measurement time.

Then, the pH influence and time dependency were evaluated by running two experiments in the presence of two different concentrations of the glucose substrate: a low level (4 x 10^{-5} M, Fig. 3C) and a high level (7 x 10^{-5} M, Fig. 3D). Standard solutions of glucose were measured every 5 min until a saturation response of the sensor was reached, where it was observed that 120 min were necessary at low concentration and 90 min at high concentration. For the lower concentration (Fig. 3C), there are two kinds of similar responses: (i) pH 5.5 and 6, and (ii) pH 7.4 and 8. At higher glucose concentrations (Fig. 3D), the response at pH 5.5 and pH 6 are significantly different, whereas at pH 5.5 the saturation was reached immediately. GOx performance is not optimal at pH values below 7.4, higher responsiveness was observed at alkaline pHs. In addition, the responses obtained at pH 7.4 and pH 8 exhibit remarkable similarity across all contact times. This can be explained by the collapsed membrane possessing the same low quantity of GOx in the Psomes membrane as validated in previous studies for various enzymes [16,18,20,32]. Consequently, prolonging the contact time consistently enhances the signal intensity regardless of pH. Furthermore, the signal variation for both concentrations remain constant across all pHs at different times. However, at a contact time of 5 min, the signal showed the highest increase for both glucose concentrations (Table S5 and S6). Therefore, the shortest contact time of 5 min was considered optimal for chronoamperometric measurements. This time should be enough to initiate and perform the desired enzymatic reactions to validate the potential of the sensing platform.

The reproducibility of the electrode modification strategy was evaluated by using four different electrodes customized using the same batch of hybrid nanomaterial. Fig. 3E presents the average of the measurements of the sensors (n = 4 sensors) for every measurement at different times (up to 60 min) in 10 mM PBS pH 7.4 and a constant concentration of glucose of 7 x 10^{-5} M. In addition, the response variation for each sensor along time (slope) was compared obtaining an average of 0.37 ± 0.05 μA min^{-1}. It can be concluded that the response patterns for all biosensors are similar.

Short-term stability was assessed by comparing the mean of measurements from all four sensors over 60 min in 10 mM PBS at pH 7.4 with a constant glucose concentration of 7 x 10^{-5} M. Low standard deviation values (Fig. 3E) in the mean measurements across the four sensors indicate stable sensor performance over time. The sensors' operational performance involves conducting 25 consecutive measurements over 120 min in the measurement medium (Fig. 3C). The modified electrode's mechanical stability was also evaluated. When stored in a refrigerator and then immersed in water, it retained stability for up to two days.

The quality parameters of the 100 % GOx-Psomes/AL sensor, including a limit of detection (LoD), limit of quantification (LoQ) and linear response range, were evaluated. The LoD and LoQ were determined using the S/N = 3 [33] and the S/N = 10 criterion, respectively.

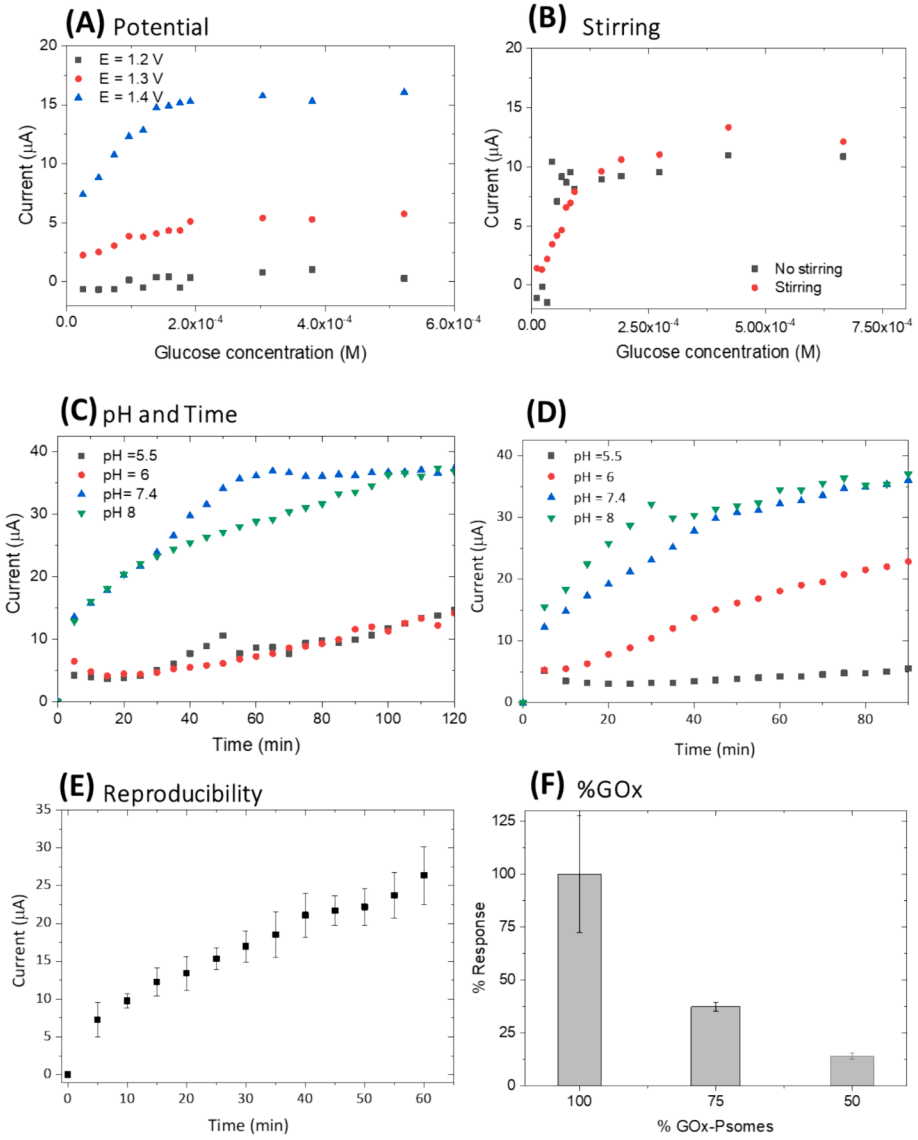

Fig. 3. Optimization of the operational electrochemical measurements for 100 % GOx-Psomes sensor. Calibration curves: (A) study of working potential; (B) evaluation of stirring effect in the measurement process. Measurements every 5 min of (C) low (4 x 10^{-5} M) and (D) high (7 x 10^{-5} M) concentration of glucose at different pH. (E) Average of the measurements along the time of four electrodes. (F) Comparison in the sensitivity for different percentages of GOx-Psomes in the modification of the electrode (n = 5 for 100 % GOx and n = 3 for 75 and 50 %). 75 % GOx-Psomes with 25 % Empty-Psomes. 50 % GOx-Psomes with 50 % Empty-Psomes.

The LoD was found to be 6 x10^{-6} M and the LoQ was found to be 3 x 10^{-5}M. The linear response range for the 100 % GOx-Psomes/AL sensor was established to be from 3 x 10^{-5} M (LoQ) to 2 x 10^{-4} M (the last glucose concentration of the linear response).

Finally, different percentages of GOx-Psomes in the hybrid nanomaterial (100, 75 and 50 %) were tested in the electrode surface modification (Table S7). The percentage response enables the comparison of the sensitivities obtained by several sensors using different composition ratios of GOx-Psomes (n = 5 for 100 % and n = 3 for 75–50 %). The 100 % GOx at pH 7.4 was used as a reference value to normalize the sensitivities. A decrease in the sensitivity of the sensors was observed in the calibration studies as the percentage of GOx-Psomes in the hybrid nanomaterial decreased (Fig. 3F) due to less H_2O_2 produced. All the data from the calibration curves are collected in Table S8.

In summary, a potential of 1.4 V with gentle continuous stirring, 10 mM PBS at pH 7.4 (closer to the physiologic pH) and with a total measurement time of 5 min are the optimal conditions for the chronoamperometric approach for monitoring the enzymatic H_2O_2 formation.

Additionally, synthetic samples were analyzed by triplicate using the optimal operation conditions. The results are gathered in Table S9 and compared with the results obtained from the average of the three measurements of the samples using the bioanalyzer YSI 2700 Select as a method of reference. The results obtained with 100 % GOx electrode (GOx-Psomes-β-CD-AuNPs@rGO/AL) are comparable to those provided by the reference method, not significant differences between both methods are obtained (95 %, $t_{cal} = 1.08 < t_{tab} = 3.18$). Intravenous glucose solution with 40 % glucose was analyzed using AuNPs@rGO/alginate and GOx-Psomes-β-CD-AuNPs@rGO/AL sensors (calibration curves were presented in Fig. S15). The results for each analysis using different sensors are summarized in Table S10.

AuNPs of AuNPs@rGO/AL sensors present non-enzymatic behavior on the oxidation of glucose. The response of the sensors in the same operational conditions does not outline the sufficient catalytic effect at pH 7.4 due to low recovery (73 ± 30 %), also observed in former studies [34,35]. On the other hand, the 100 % GOx-Psomes electrode shows an

enhanced and constant response compared with the reference method and the recovery is improved (89 ± 2 %) compared with only AuNPs modified electrode. This also implies a reproducible incorporation of all components (GOx-Psomes and AuNPs@rGO) in the AL matrix on hand-made electrode surface modification.

3.5. Proof of concept of a cascade reaction on the biosensor surface

Finally, a cascade enzymatic reaction can be investigated as an intermolecular communication through the diffusion of metabolites between two differently loaded Psomes (Scheme 1B) under low current conditions. This advancement can lead to the development of novel sensing approaches with enhanced selectivity. To investigate this, two different nanocompartments (GOx-Psomes and CAT-Psomes, heterogeneous cargo) were incorporated into the AL network on the electrode surfaces. In addition, $(\beta CD)_2$Hemin-Psomes as NZs were studied as an analogue to CAT-Psomes as NEs (Scheme 1B) due to the superior structural and functional robustness of NZs.

Fig. 4 illustrates the distinct behaviors of modified electrodes. In Fig. 4A, the sensor "100 % GOx-Psomes" exhibits the highest current at a low glucose concentration (4 x 10^{-5} M) at pH 7.4, reflecting its high H_2O_2 production. For "50 % GOx-Psomes", a decrease in current is observed due to reduced H_2O_2 production. Sensors "50 % CAT- and $(\beta CD)_2$Hemin-Psomes" incorporate a heterogenous cargo in the AL network, demonstrating similar catalytic activity for H_2O_2 consumption. This leads to comparable lower currents compared to 100 % and 50 % GOx-Psomes, which are responsible for H_2O_2 production. Therefore, the lower current detected by 50 % CAT- and $(\beta CD)_2$Hemin-Psomes is attributed to H_2O_2 consumption as a counterpart to GOx-Psomes in the AL matrix.

Furthermore, at pH 6, the cascade reaction of NEs (CAT) and NZs ($(\beta CD)_2$Hemin) were studied to compare the results at pH 7.4, using the same glucose concentration (Fig. 4B). Surprisingly, no difference in the response to both sensors is observed. It is important to highlight that due to the characteristics of the NZs, higher stability and cost-effectiveness, another ratio is tested (90 % Hemin complex) and differences in the performance depending on the pH (Fig. 4C) were obtained. At pH 6 the efficiency of $(\beta CD)_2$Hemin seems better than at pH 7.4. Due to the swollen state of $(\beta CD)_2$Hemin-Psomes (Fig. S2), there is a higher permeability of H_2O_2 through the swollen Psomes membrane into the lumen of $(\beta CD)_2$Hemin-Psomes where the most NZs are located known from a previous study [21].

The study of the sensitivity of the calibration curves performed using different sensors is presented in Fig. 4D to validate the influence of NEs and NZs on GOx-Psomes activity at pH 7.4 and 6 in a changing environment within the AL matrix on the electrode surface. The data of the calibration curves is summarized in Table S8. The results were normalized against the response of 100 % GOx electrodes, setting their response (current) at each pH to 100 %. The 100 % GOx sensor exhibits a pH-dependent gap in its response, with an average sensitivity of 32974 ± 7927 μA M^{-1} at pH 6 and 123267 ± 34040 μA M^{-1} at pH 7.4. This difference in sensitivity is attributed to the optimum pH of GOx, which is 7.4, where it produces the highest amount of H_2O_2. The experimental uncertainty observed is compensated by repeating the experiment whereby the measurements were performed in quintuplicate (100 % GOx-Psomes) and triplicate (50 % CAT-Psomes and 90 and 50 %

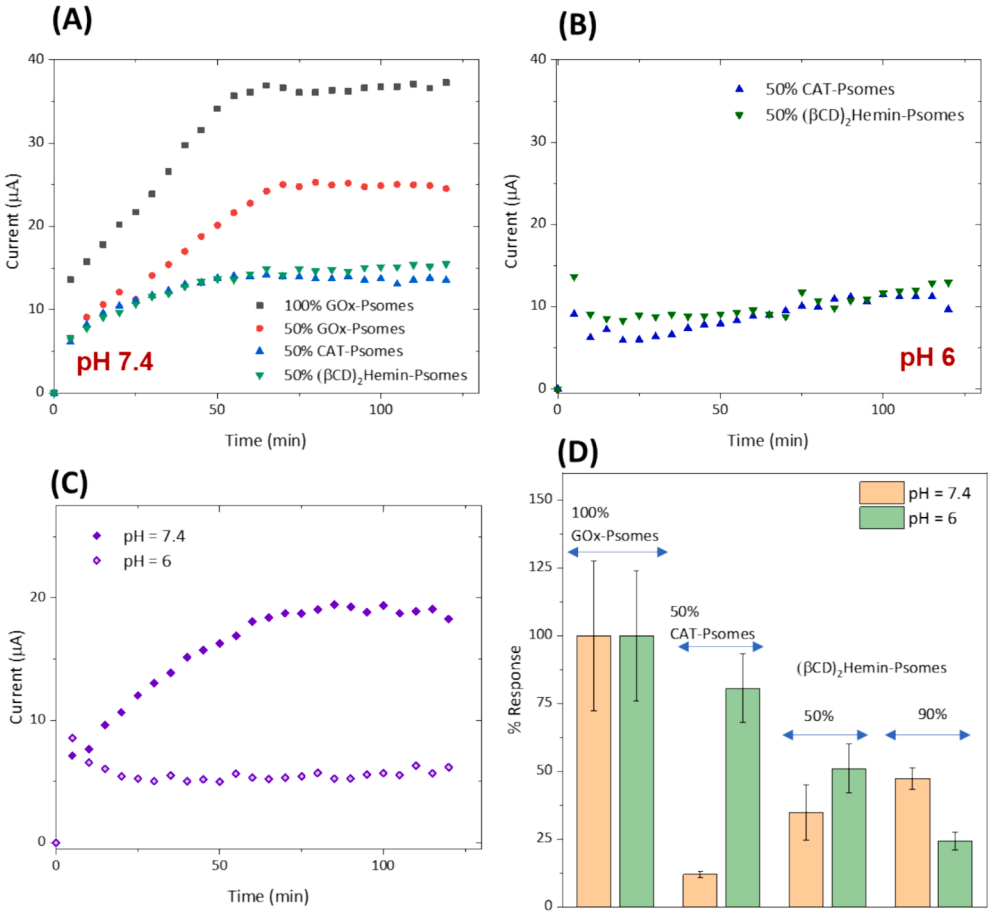

Fig. 4. Evolution of the measurement of (A) 4 x 10^{-5} M glucose at pH = 7.4; (B) 4 x 10^{-5} M glucose at pH = 6 (C) 4 x 10^{-5} M glucose at pH = 6 and 7.4 for 90 % $(\beta CD)_2$Hemin-Psomes sensors (D) comparison of the % Response obtained (n = 3 except n (100 % GOx-Psomes, 7.4) = 5). *Experimental conditions:* 1.4 V, 5 min between measurements, stirring and pH 7.4. Error in the measurements ≤ 5 μA.

(βCD)$_2$Hemin-Psomes) using different hand-made sensors.

The percentage response of the 50 % (βCD)$_2$Hemin-Psomes sensor at pH 7.4 is slightly higher than that obtained with the 50 % CAT-Psomes sensor at the same pH containing the same amount of NE (GOx). This implies that this pH is not optimum to the (βCD)$_2$Hemin or the feeding is retarded due to their location in the polymeric nanoreactor [21]. Independent of the loading efficiency of NEs and NZs in Psomes (CAT (~0.05 μM, 250 kDa) 30 times less than that of (βCD)$_2$-Hemin (~1.5 μM, 3 kDa)), it is assumed that CAT biomacromolecules must be integrated into the collapsed Psomes membrane at pH 7.4, and, therefore, free feeding of CAT with H_2O_2 is possible. Contrary, there are few integrated (βCD)$_2$Hemin in the collapsed Psomes membrane [21] where there is a retarded feeding of NZs with H_2O_2 in (βCD)$_2$Hemin-Psomes compared to pH 6. Overall, the results of the enzymatic cascade reaction undoubtedly show that NZs can serve as a more affordable alternative to NEs, particularly when NZs are freely fed within a defined confinement. However, further targeted experiments are warranted to elucidate the somewhat contradictory findings observed for 50 % and 90 % (βCD)$_2$Hemin-Psomes at pH 7.4 in the future.

4. Conclusions

The surface modification strategy of composite electrodes based on biocompatible carbon materials with integrated reduced graphene oxide-gold nanoparticles hybrid materials in a cross-linked alginate matrix containing polymeric nanoreactors leads a sensing platform with applications beyond a biosensor, targeted at monitoring more complex reactions occurring in nature. Here, we have demonstrated the potential of loaded NZs and NEs in the protective environment of polymeric vesicles (Psomes) in molecular communication by outlining pH-dependent enzymatic(−like) activities. These biologically active core-loaded nanoreactors can be smoothly integrated into the alginate matrix with different composition mixtures promoting different rates of substrate consumption.

As a proof of concept, the study successfully demonstrated the compartmentalization of natural model enzymes such as GOx (H_2O_2-producing) and CAT (H_2O_2-consuming). This showcased the feasibility of altering the electrode by incorporating heterogeneously bioactive cargo within an alginate matrix, while also establishing effective communication between these enzymatic counterparts. In addition, the potential of using NZs such as a Hemin complex as a substitute for peroxide consumption has been verified. The benefit of NZs towards NEs is their higher stability over time and the reduction in the cost to fabricate them. This presents a novel approach for the development of customized sensors with highlighted sensing capabilities. On the one hand, Psomes exhibit a high level of sophistication as nanocompartments, enabling them to seamlessly integrate both NEs and NZs, thus ensuring robust protection for each component. This capability can potentially be expanded to encompass a wide range of other biologically active cavities (natural or artificial), which can be triggered by various stimuli. Furthermore, heterogeneous incorporation and effective communication between these polymeric nanocompartments are also achievable. This breakthrough paves the way for the exploration of more intricate biological processes, such as intercellular compartment communication, using analytical platforms equipped with versatile and adjustable detection capabilities.

CRediT authorship contribution statement

Laia L. Fernández: Writing – original draft, Investigation. **Julio Bastos-Arrieta:** Writing – review & editing, Supervision, Investigation. **Dietmar Appelhans:** Writing – review & editing, Supervision. **Yang Zhou:** Investigation. **Silvia Moreno:** Writing – review & editing, Writing – original draft, Supervision, Investigation, Conceptualization. **Cristina Palet:** Writing – review & editing, Supervision. **Mireia Baeza:** Writing – review & editing, Writing – original draft, Supervision, Project administration, Funding acquisition, Conceptualization.

Declaration of competing interest

The authors declare that they have no known competing financial interests or personal relationships that could have appeared to influence the work reported in this paper.

Data availability

The data presented in this study are available on request to the corresponding authors. The data are not publicly available because the repository that is used to keep the data is a private one provided by the University.

Acknowledgements

Laia L. Fernández acknowledges Universitat Autónoma de Barcelona (UAB) for the PIF grant and the authors acknowledge Servei de Microscopia of UAB for the SEM, TEM and EDX analysis. Mr. Andreas Schurig for the synthesis of BCPs. Ms. Alissa Seifert for GPC measurements. Ms. Franzisca Kucharczyk for supporting the reproducibility of some experiments. Authors acknowledge the grant PID2021-126253OB-C21 funded by MCIN/AEI/10.13039/501100011033 and by "ERDF A way of making Europe", by the "European Union", for the financial support provided to perform this research.

Appendix A. Supplementary data

Supplementary data to this article can be found online at https://doi.org/10.1016/j.microc.2024.111071.

References

[1] G. Rocchitta, A. Spanu, S. Babudieri, G. Latte, G. Madeddu, G. Galleri, S. Nuvoli, P. Bagella, M.I. Demartis, V. Fiore, R. Manetti, P.A. Serra, Enzyme biosensors for biomedical applications: strategies for safeguarding analytical performances in biological fluids, Sensors (switzerland) 16 (6) (2016), https://doi.org/10.3390/s16060780.

[2] J. Bastos-Arrieta, R. Montes, C. Ocaña, M. Espinoza, M. Muñoz, M. Baeza, In situ characterization of size, spatial distribution, chemical composition, and electroanalytical response of hybrid nanocomposite materials, in: C. Kumar (Ed.), In-Situ Characterization Techniques for Nanomaterials, Springer, Berlin, Heidelberg, 2018, https://doi.org/10.1007/978-3-662-56322-9_8.

[3] R. Montes, F. Céspedes, M. Baeza, Highly sensitive electrochemical immunosensor for IgG detection based on optimized rigid biocomposites, Biosens Bioelectron 78 (2016) 505–512, https://doi.org/10.1016/j.bios.2015.11.081.

[4] R. Montes, J. Bartrolí, F. Céspedes, M. Baeza, Towards to the improvement of the analytical response in voltammetric sensors based on rigid composites, J. Electroanal. Chem. 733 (2014) 69–76, https://doi.org/10.1016/j.jelechem.2014.09.022.

[5] F. Mazur, M. Bally, B. Städler, R. Chandrawati, Liposomes and lipid bilayers in biosensors, Adv Colloid Interface Sci 249 (2017) 88–99, https://doi.org/10.1016/j.cis.2017.05.020.

[6] X. Hu, Y. Zhang, Z. Xie, X. Jing, A. Bellotti, Z. Gu, Stimuli-responsive polymersomes for biomedical applications, Biomacromolecules 18 (3) (2017) 649–673, https://doi.org/10.1021/acs.biomac.6b01704.

[7] E. Rideau, R. Dimova, P. Schwille, F.R. Wurm, K. Landfester, Liposomes and polymersomes: a comparative review towards cell mimicking, Chem Soc Rev 47 (2018) 8572–8610, https://doi.org/10.1039/c8cs00162f.

[8] M.V. Dinu, I.A. Dinu, S.S. Saxer, W. Meier, U. Pieles, N. Bruns, Stabilizing enzymes within polymersomes by coencapsulation of trehalose, Biomacromolecules 22 (1) (2021) 134–145, https://doi.org/10.1021/acs.biomac.0c00824.

[9] O. Rifaie-Graham, J. Yeow, A. Najer, R. Wang, R. Sun, K. Zhou, T.N. Dell, C. Adrianus, C. Thanapongpibul, M. Chami, S. Mann, J.R. de Alaniz, M.M. Stevens, Photoswitchable gating of non-equilibrium enzymatic feedback in chemically communicating polymersome nanoreactors, Nat Chem 15 (2023) 110–118, https://doi.org/10.1038/s41557-022-01062-4.

[10] H. Che, J.C.M. Van Hest, Stimuli-responsive polymersomes and nanoreactors, J Mater Chem B 4 (2016) 4632–4647, https://doi.org/10.1039/c6tb01163b.

[11] M. El Idrissi, C.E. Meyer, L. Zartner, W. Meier, Nanosensors based on polymer vesicles and planar membranes: a short review, J Nanobiotechnology 16 (2018) 63, https://doi.org/10.1186/s12951-018-0393-7.

[12] A. Mohammadpour-Haratbar, Y. Zare, K.Y. Rhee, Electrochemical biosensors based on polymer nanocomposites for detecting breast cancer: recent progress and future

prospects, Adv Colloid Interface Sci 309 (2022) 102795, https://doi.org/10.1016/j.cis.2022.102795.
[13] N. Anzar, R. Hasan, M. Tyagi, N. Yadav, J. Narang, Carbon nanotube - a review on synthesis, properties and plethora of applications in the field of biomedical science, Sensors International 1 (2020) 100003, https://doi.org/10.1016/j.sintl.2020.100003.
[14] V. Gurylev, T.K. Chin, H.Y. Tsai, Carbon nanotubes decorated with platinum nanoparticles for field-emission application, ACS Omega 4 (13) (2019) 15428–15434, https://doi.org/10.1021/acsomega.9b01478.
[15] C. Tan, X. Huang, H. Zhang, Synthesis and applications of graphene-based noble metal nanostructures, Mater. Today 16 (1–2) (2013) 29–36, https://doi.org/10.1016/j.mattod.2013.01.021.
[16] K. Zhang, S. Moreno, X. Wang, Y. Zhou, S. Boye, D. Voigt, B. Voit, D. Appelhans, Biomimetic cell structures: probing induced pH-feedback loops and pH self-monitoring in cytosol using binary enzyme-loaded polymersomes in proteinosome, Biomacromolecules 24 (6) (2023) 2489–2500, https://doi.org/10.1021/acs.biomac.3c00010.
[17] D. Gräfe, J. Gaitzsch, D. Appelhans, B. Voit, Cross-linked polymersomes as nanoreactors for controlled and stabilized single and cascade enzymatic reactions, Nanoscale 6 (2014) 10752–10761, https://doi.org/10.1039/c4nr02155j.
[18] S. Moreno, P. Sharan, J. Engelke, H. Gumz, S. Boye, U. Oertel, P. Wang, S. Banerjee, R. Klajn, B. Voit, A. Lederer, D. Appelhans, Light-driven proton transfer for cyclic and temporal switching of enzymatic nanoreactors, Small 16 (37) (2020) 2002135, https://doi.org/10.1002/smll.202002135.
[19] P. Wang, S. Moreno, A. Janke, S. Boye, D. Wang, S. Schwarz, B. Voit, D. Appelhans, Probing crowdedness of artificial organelles by clustering polymersomes for spatially controlled and pH-triggered enzymatic reactions, Biomacromolecules 23 (9) (2022) 3648–3662, https://doi.org/10.1021/acs.biomac.2c00546.
[20] D. Wang, S. Moreno, M. Gao, J. Guo, B. Xu, D. Voigt, B. Voit, D. Appelhans, Protocells capable of generating a cytoskeleton-like structure from intracellular membrane-active artificial organelles, Adv Funct Mater 33 (50) (2023) 2306904, https://doi.org/10.1002/adfm.202306904.
[21] S. Moreno, S. Alex, L.L. Fernandez, U. Lappan, S. Boye, B. Voit, D. Appelhans, Peroxidase-mimicking activity of nanozymes-loaded polymeric artificial organelles potentially active in acidic environment, J. Polym. Sci. 61 (16) (2023) 1859–1869, https://doi.org/10.1002/pol.20230100.
[22] F. Rajabasadi, S. Moreno, K. Fichna, A. Aziz, D. Appelhans, O.G. Schmidt, M. Medina-Sánchez, Multifunctional 4D-printed sperm-hybrid microcarriers for assisted reproduction, Adv. Mater. 34 (50) (2022) 2204257, https://doi.org/10.1002/adma.202204257.
[23] J. Gaitzsch, D. Appelhans, L. Wang, G. Battaglia, B. Voit, Synthetic bio-nanoreactor: mechanical and chemical control of polymersome membrane permeability, Angew. Chem. Int. Ed. 51 (18) (2012) 4448–4451, https://doi.org/10.1002/anie.201108814.
[24] J. Muñoz, M. Riba-Moliner, L.J. Brennan, Y.K. Gun'ko, F. Céspedes, A. González-Campo, M. Baeza, Amperometric thyroxine sensor using a nanocomposite based on graphene modified with gold nanoparticles carrying a thiolated β-cyclodextrin, Microchim. Acta 183 (2016) 1579–1589, https://doi.org/10.1007/s00604-016-1783-x.
[25] P. Sánchez-Peña, J. Rodriguez, D. Gabriel, J.A. Baeza, A. Guisasola, M. Baeza, Graphene functionalization with metallic Pt nanoparticles: a path to cost-efficient H_2 production in microbial electrolysis cells, Int J Hydrogen Energy 47 (34) (2022) 15397–15409, https://doi.org/10.1016/j.ijhydene.2022.03.078.
[26] A. Schmitt, P. Rödel, C. Anamur, C. Seeliger, A.B. Imhoff, E. Herbst, S. Vogt, M. Van Griensven, G. Winter, J. Engert, Calcium alginate gels as stem cell matrix -making paracrine stem cell activity available for enhanced healing after surgery, PLoS One 10 (2015), https://doi.org/10.1371/journal.pone.0118937.
[27] E. Forner, J.J. Ezenarro, M. Pérez-Montero, N. Vigués, A. Asensio-Grau, A. Andrés, J. Mas, M. Baeza, X. Muñoz-Berbel, R. Villa, G. Gabriel, Electrochemical biosensor for aerobic acetate detection, Talanta 265 (2023) 124882, https://doi.org/10.1016/j.talanta.2023.124882.
[28] D. Wang, S. Moreno, S. Boye, B. Voit, D. Appelhans, Detection of subtle extracellular glucose changes by artificial organelles in protocells, Chem. Commun. 57 (2021) 8019–8022, https://doi.org/10.1039/d1cc03422g.
[29] X. Wang, S. Moreno, S. Boye, P. Wen, K. Zhang, P. Formanek, A. Lederer, B. Voit, D. Appelhans, Feedback-induced and oscillating pH regulation of a binary enzyme-polymersomes system, Chem. Mater. 33 (17) (2021) 6692–6700, https://doi.org/10.1021/acs.chemmater.1c00897.
[30] K. Rudnicki, M. Brycht, A. Leniart, S. Domagała, K. Kaczmarek, K. Kalcher, S. Skrzypek, A sensitive sensor based on single-walled carbon nanotubes: its preparation, characterization and application in the electrochemical determination of drug clorsulon in milk samples, Electroanalysis 32 (2) (2020) 375–383, https://doi.org/10.1002/elan.201900387.
[31] C.T.T. Thuy, J.Y. Park, S.W. Lee, T. Suresh, J.H. Kim, Surfactant effect in polypyrrole and polypyrrole with multi wall carbon nanotube counter electrodes: improved power conversion efficiency of dye-sensitized solar cell, J Nanosci Nanotechnol 16 (5) (2016) 5263–5267, https://doi.org/10.1166/jnn.2016.12266.
[32] X. Wang, S. Moreno, S. Boye, P. Wang, X. Liu, A. Lederer, B. Voit, D. Appelhans, Artificial organelles with orthogonal-responsive membranes for protocell systems: probing the intrinsic and sequential docking and diffusion of cargo into two coexisting avidin-polymersomes, Adv. Sci. 8 (11) (2021) 2004263, https://doi.org/10.1002/advs.202004263.
[33] A. Shrivastava, V. Gupta, Methods for the determination of limit of detection and limit of quantitation of the analytical methods, Chronicles of Young Scientists 2 (1) (2011) 21–25, https://doi.org/10.4103/2229-5186.79345.
[34] M. Sharifi, K. Faryabi, A.J. Talaei, M.S. Shekha, M. Ale-Ebrahim, A. Salihi, N.M. Q. Nanakali, F.M. Aziz, B. Rasti, A. Hasan, M. Falahati, Antioxidant properties of gold nanozyme: a review, J Mol Liq 297 (2020) 112004, https://doi.org/10.1016/j.molliq.2019.112004.
[35] X. Wang, W. Guo, Y. Hu, J. Wu, H. Wei, Nanozymes: Next Wave of Artificial Enzymes, SpringerBriefs in Molecular Science, Springer, Berlin, Heidelberg, eBook, Series Title, 2016.